Ultra-sensitive uric acid second generation biosensor based on chemical immobilization of uricase on functionalized multiwall carbon nanotube grafted palm oil fiber in the presence of ferrocene mediator

Gullit Deffo [a, b], Ranjit Hazarika [a], Marcel Cédric Deussi Ngaha [b, c], Mwina Basumatary [a], Shyamali Kalita [a], Nayab Hussain [a], Evangéline Njanja [b], Panchanan Puzari [a] *, Emmanuel Ngameni [d].

[a] *Department of Chemical Sciences, Tezpur University, Tezpur, Assam 784028, India.*

[b]*Electrochemistry and Chemistry of Materials, Department of Chemistry, Faculty of Science, University of Dschang, P.O. Box 67, Dschang, Cameroon.*

[c]*Department of Chemistry, Higher Teacher Training College, University of Bamenda, Bambili P.O.Box. 39, Cameroon.*

[d]*Laboratory of Analytical Chemistry, Department of Chemistry, University of Yaoundé 1, P.O. Box 812, Yaoundé, Cameroon.*

* Corresponding author. *E-mail address:* pancha@tezu.ernet.in (P. Puzari)

Supporting Information

SC-1. FMWCNT-POF grafting procedure

The synthetic route of FMWCNT-POF is shown by scheme SC1.

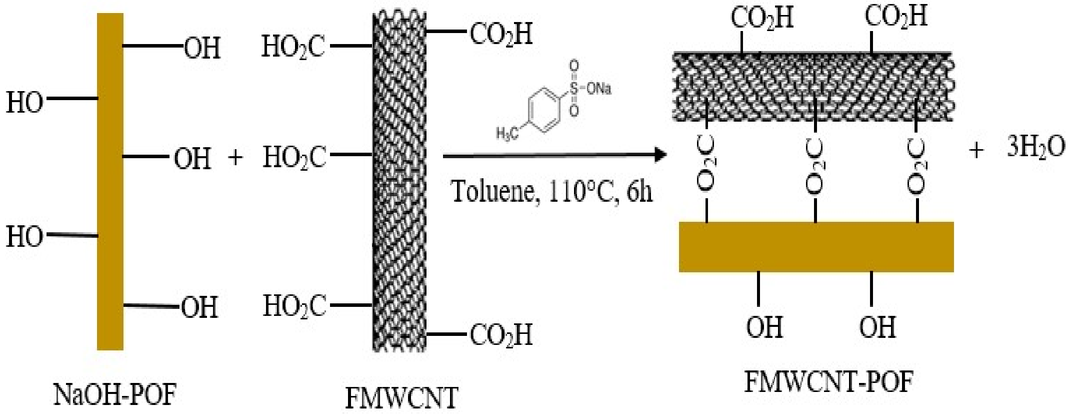

Scheme SC1. Grafting FMWCNT onto NaOH-POF.

SF1-. UV-vis of UA and UOx

From figure SF1A, it can be seen that the absorbance of UA (prepared in phosphate buffer pH 7) decrease rapidly in the presence of UOx for the first 60 s, and start decrease slowly from 120 s as clearly represented by the histogram of figure SF1B. The plot of unit activity of enzyme versus the time show by figure SF1 was established by using the equation (1)[1].

$$Unit\ activity = \frac{(\Delta A_{293}\ in\ test\ solution - blank)\ x\ test\ volume}{12.6\ x\ volume\ of\ enzyme\ taken} \qquad \text{(S1)}$$

Where ΔA is the change in absorbance at 293 nm, blank (no UOx) is the mixture of 2970 µL of TB (pH 8.5) with 30 µL of UA (0.1 M), test volume is the mixture of 2970 µL of TB (pH 8.5), 30 µL of UA (0.1 M) and 100 µL of UOx (1 mg/ml), 12.6 is the extinction coefficient of UA and volume of enzyme taken = 100 µL.

This result justifying the fast reactivity of UOx in contact with UA, therefore can be immobilize on the electrode for the elaboration of the UA biosensor.

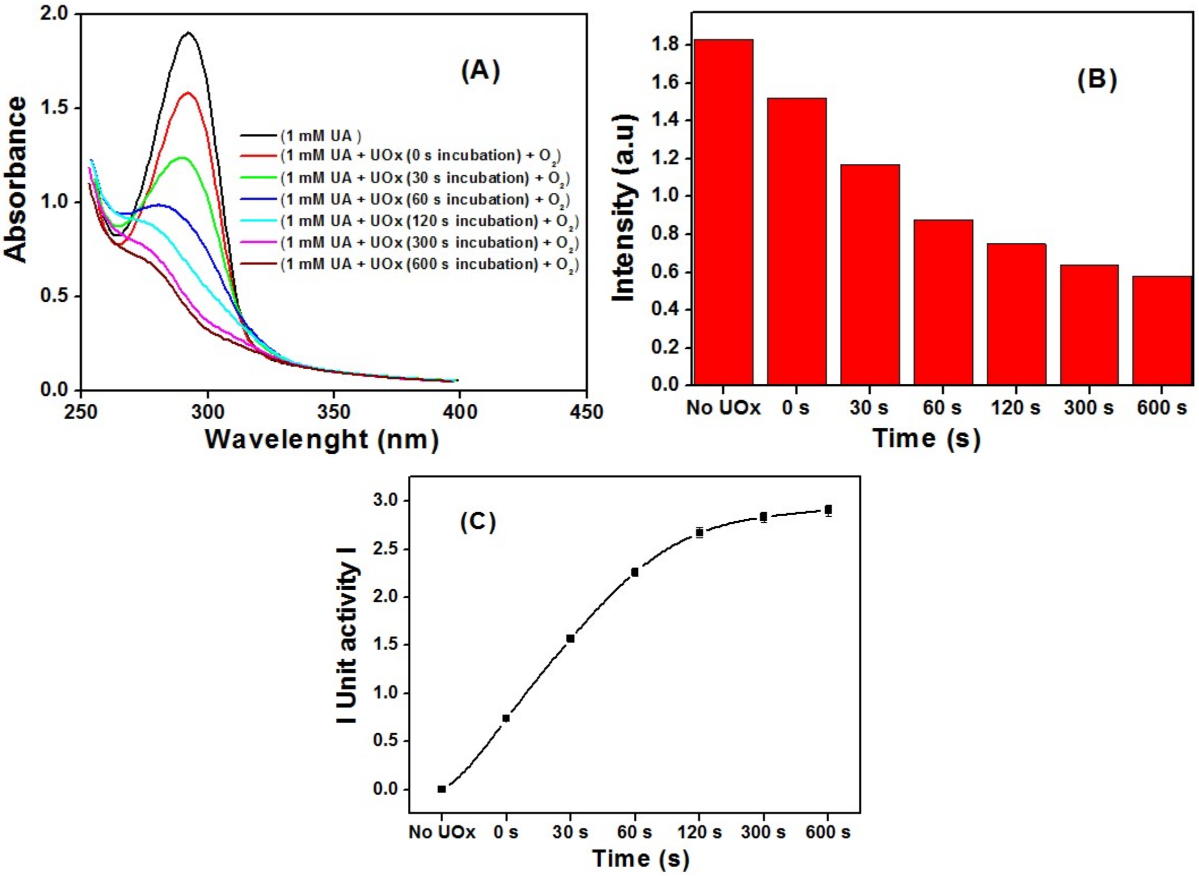

Fig. SF1. (A) UV-vis spectrum of uric acid (UA) without and with uricase (UOx); (B) Histogram showing the corresponding intensity. (C) The plot of unit activity against the time.

SF2. Thermal Analysis of NaOH-POF, FMWCNT, and FMWCNT-POF

The thermogravimetric (TG) plot of NaOH-POF (Figure SF2A), show four weight losses from: 40°C to 96°C (10.89%); 224°C to 305°C (69.54%); 306 to 415°C (12.38%) and 420°C to 444°C (1.01%) which correspond respectively to the loss of water molecule, destruction of hemicelluose, decomposition of cellulose, and decomposition of lignin[2]. TG plot of FMWCNT (Figure SF2B) show two weight losses: the first one from 154°C to 222°C (4.96%) which correspond to the degradation of carboxylic acid grafted on MWCNT, and the second one from 570 °C which correspond to the degradation of the material MWCNT[3-4]. Figure SF2C showing the TG plot of FMWCNT-POF present five distinct weight losses, where the first loss occurring between 45°C to 83°C (1.09 %) is assigned to the departure of molecule of water. The second weight loss between 172°C to 332°C (45.991%) is related to the destruction of hemicelluloses and the chemical bond between FMWCNT and POF. The third one from 377°C to 484°C (16.389 %) is assigned to the destruction of cellulose. The four weight loss between 553°C to 600°C correspond to the decomposition of lignin whereas the last one from 614°C is assigned to the decomposition of MWCNT.

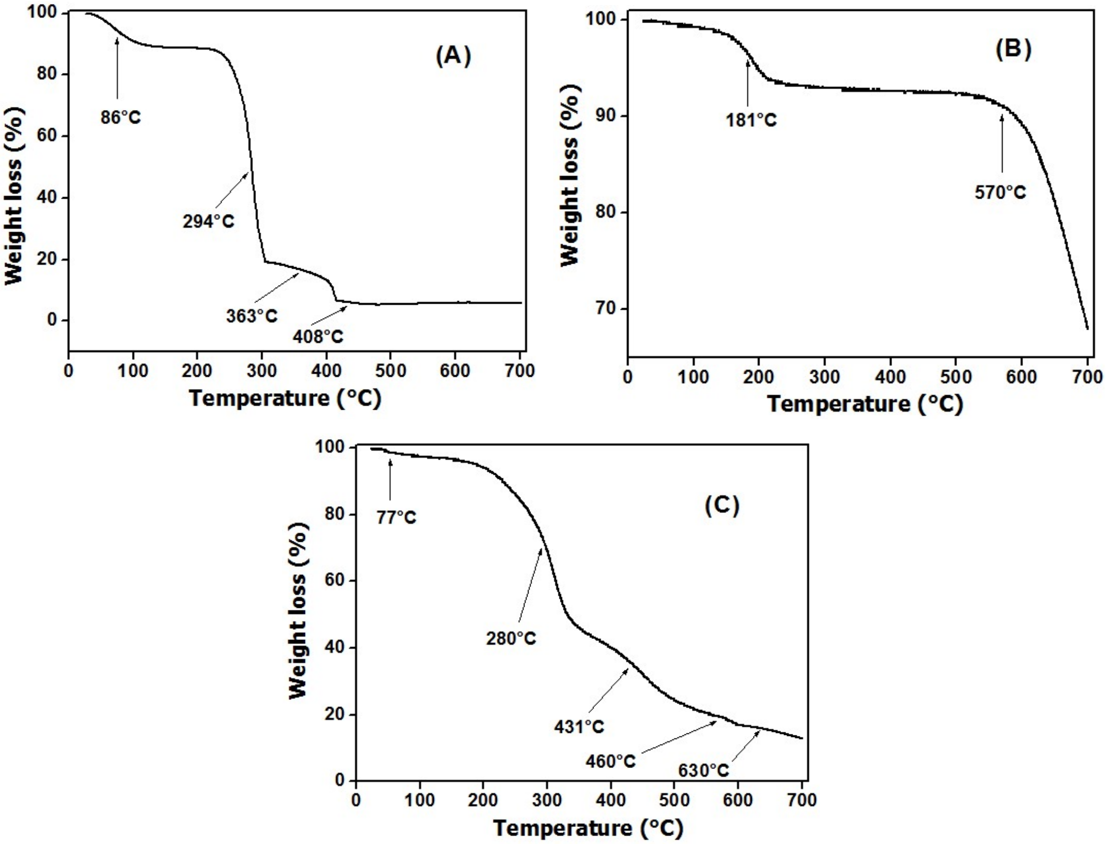

Fig. SF2. TG curves of (A) NaOH-POF, (B) FMWCNT, (C) FMWCNT-POF.

SF3. Transmission electron microscopy of MWCNT, FMWCNT, FMWCNT-POF, and Fc/FMWCNT-POF

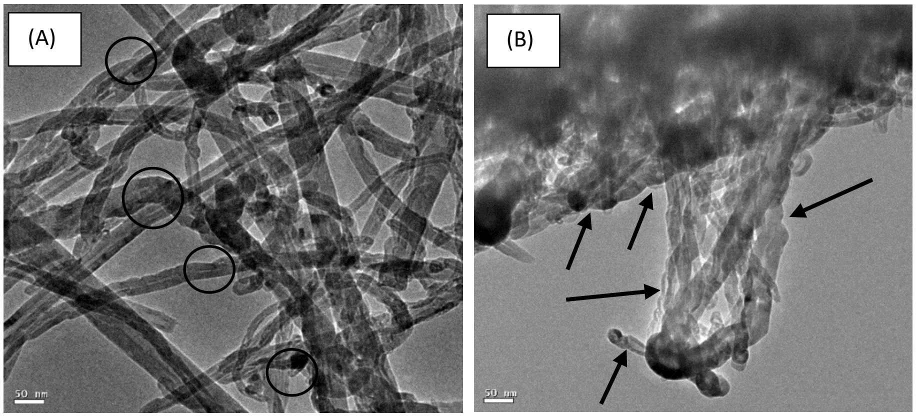

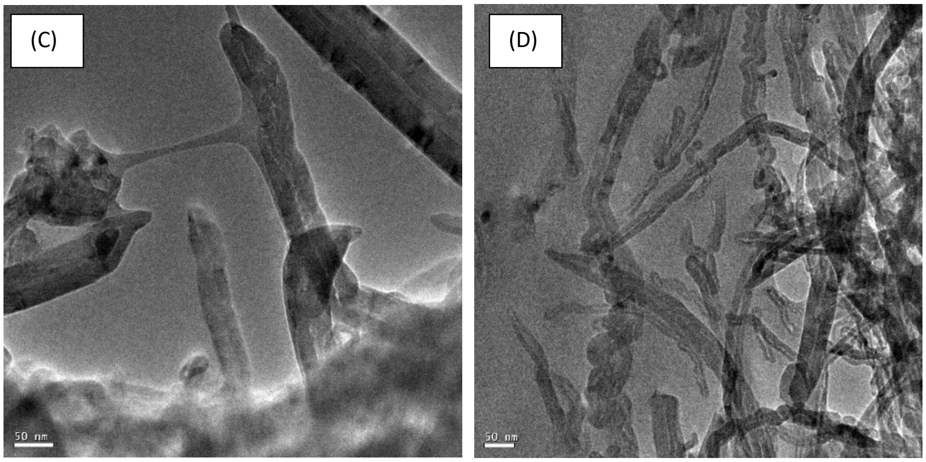

Fig. SF3. TEM images of (A) MWCNT, (B) FMWCNT, (C) FMWCNT-POF, and (D) Fc/FMWCNT-POF

SF4. Energy dispersive X-ray analysis of MWCNT, FMWCNT, FMWCNT-POF, and Fc/FMWCNT-POF

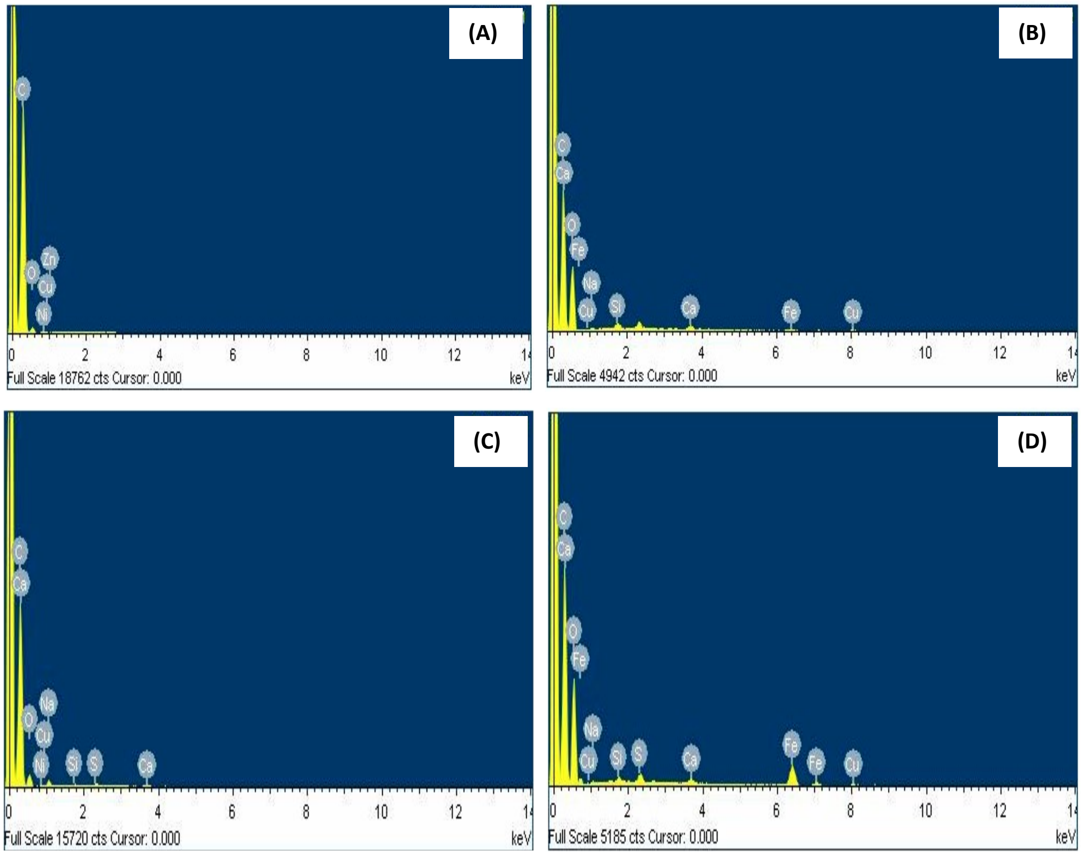

Fig. SF4. EDX images of (A) MWCNT, (B) FMWCNT, (C) FMWCNT-POF, and (D) Fc/FMWCNT-POF

Table ST1. EDX data (weight %) of MWCNT, FMWCNT, FMWCNT-POF, and Fc/FMWCNT-POF.

Materials	C (%)	O (%)	Ni (%)	Cu (%)	Zn (%)	Na (%)	Ca (%)	Fe (%)	S (%)
MWCNT	86.30	12.02	0.73	0.50	0.45	/	/	/	/
FMWCNT	51.05	45.64	/	1.02	/	0.47	0.69	0.61	/
FMWCNT-POF	49.95	42.68	/	0.66	/	1.43	0.24	0.35	0.39
Fc/FMWCNT-POF	79.95	18.64	/	0.50	/	0.29	0.24	5.24	0.63

Table ST2 and ST3: Elemental Analysis (EA) and BET analysis of POF and NaOH-POF

Table ST2 show the reduction in the percentage of the elements occurred after alkali activation of the POF. It can be seen from the BET analysis data (table ST3) that after conversion to NaOH-POF, the active surface was increased and a better porosity was achieved.

Table ST2. EA of raw POF and NaOH-POF.

Materials	C (%)	H (%)	N (%)
Raw POF	42.282	6.276	0.788
NaOH-POF	40.532	6.161	0.263

Table ST3. Nitrogen adsorption-desorption of raw POF and NaOH-POF.

Materials	BET surface area ($m^{-2}.g^{-1}$)	Pore volumes ($cm^3.g^{-1}$)	Mesopores volume ($cm^3.g^{-1}$)	Mesopores surface ($m^{-2}.g^{-1}$)	Micropores volume ($cm^3.g^{-1}$)	Micropores surface ($m^{-2}.g^{-1}$)
Raw POF	287.080	0.242	0.232	186.510	0.091	94.209
NaOH-POF	349.770	0.293	0.304	234.270	0.102	106.490

SF5. Effect of scan rate on Fc/FMWCNT-POF/Pt and UOx/Fc/FMWCNT-POF/Pt and activity of ferrocene

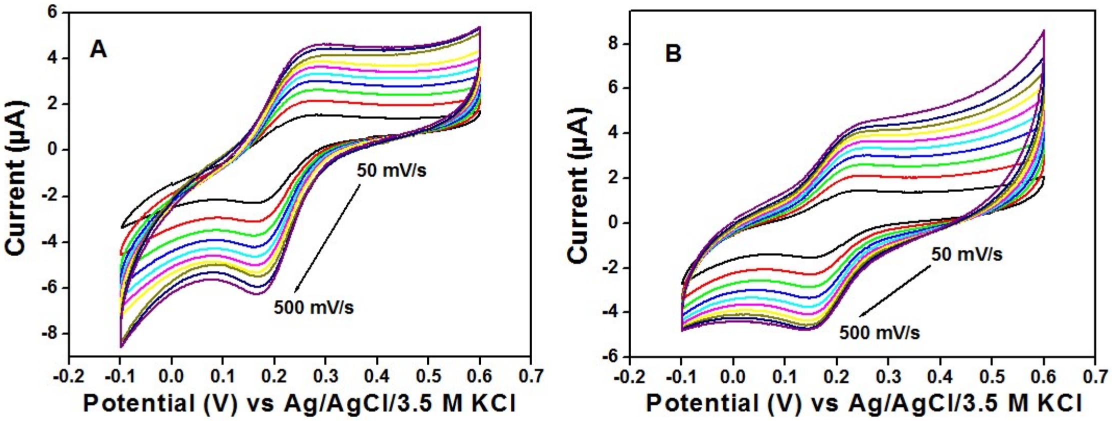

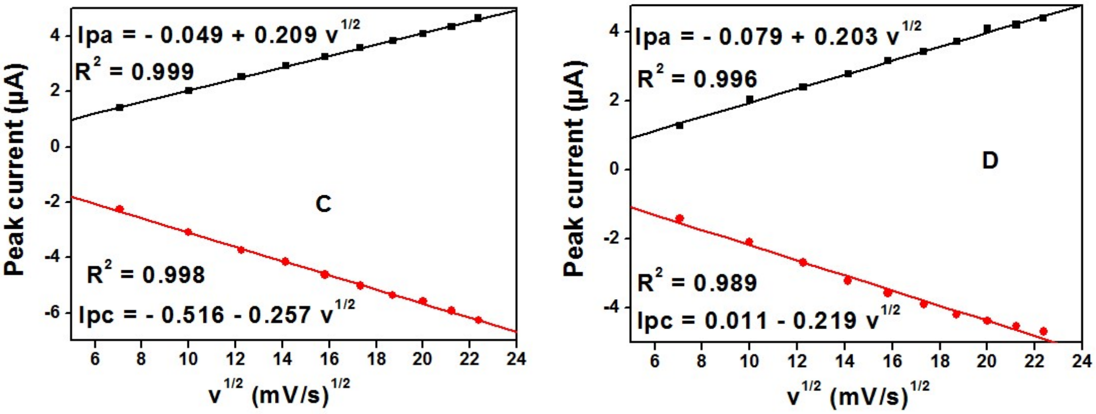

Fig. SF5. Multisweep cyclic voltammograms (A and B) and the corresponding peak currents versus the root square of the scan rate (C and D) respectively for Fc/FMWCNT-POF/Pt and UOx/Fc/FMWCNT-POF/Pt recorded in 0.1 M KCl at pH 7. The scan rate was 50; 100; 150; 200; 250; 300; 350; 400; 450 and 500 mV/s.

SF6. Active surface of bare Pt, Fc/FMWCNT-POF/Pt and UOx/Fc/FMWCNT-POF/Pt

From figure S6A, B, and C, it can be seen that the peak currents of the reversible system increase with the scan rate for each electrode showing the increase of the redox activity. The Ipa and Ipc values were plotted against $v^{1/2}$ for each electrode as shown in figure S6D, E, and F. A linear regression is obtained in each cases with good correlation coefficient close to 1, justifying a diffusion controlled process at the electrode-electrolyte interface[5-6]. Therefore, the value of the active surface can be determine using the Randles-Sevcik equation (equation S2).

$$I_p = Kn^{\frac{3}{2}}AD^{\frac{1}{2}}Cv^{\frac{1}{2}} \qquad \text{(S2)}$$

with the constant K = 2.09 x 10^5, the number of electron exchanged n = 1, the concentration of the analyte C = 5 mM, the real surface (cm^2) A, the scan rate v, the diffusion coefficient D = 7.6 x 10^{-6} cm^2/s.

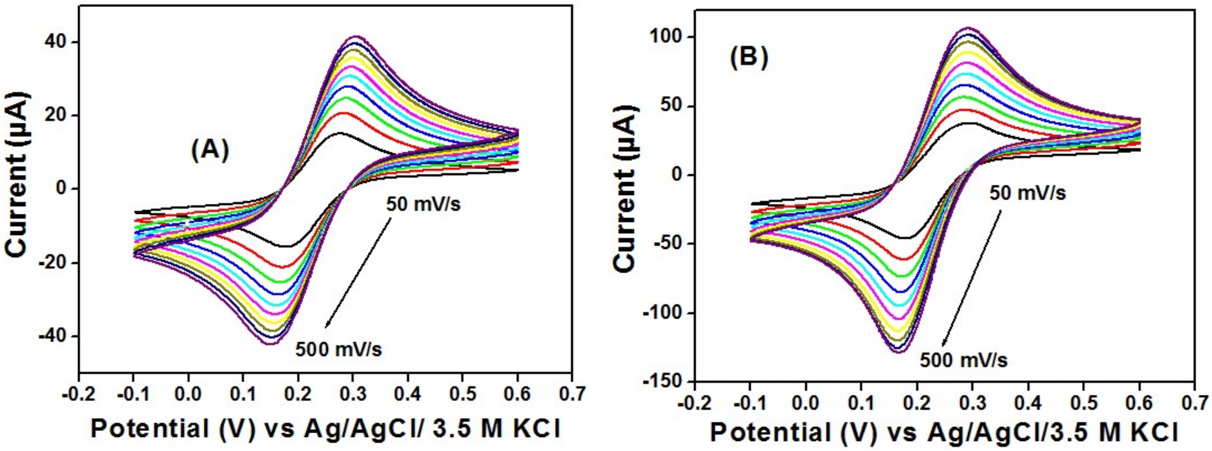

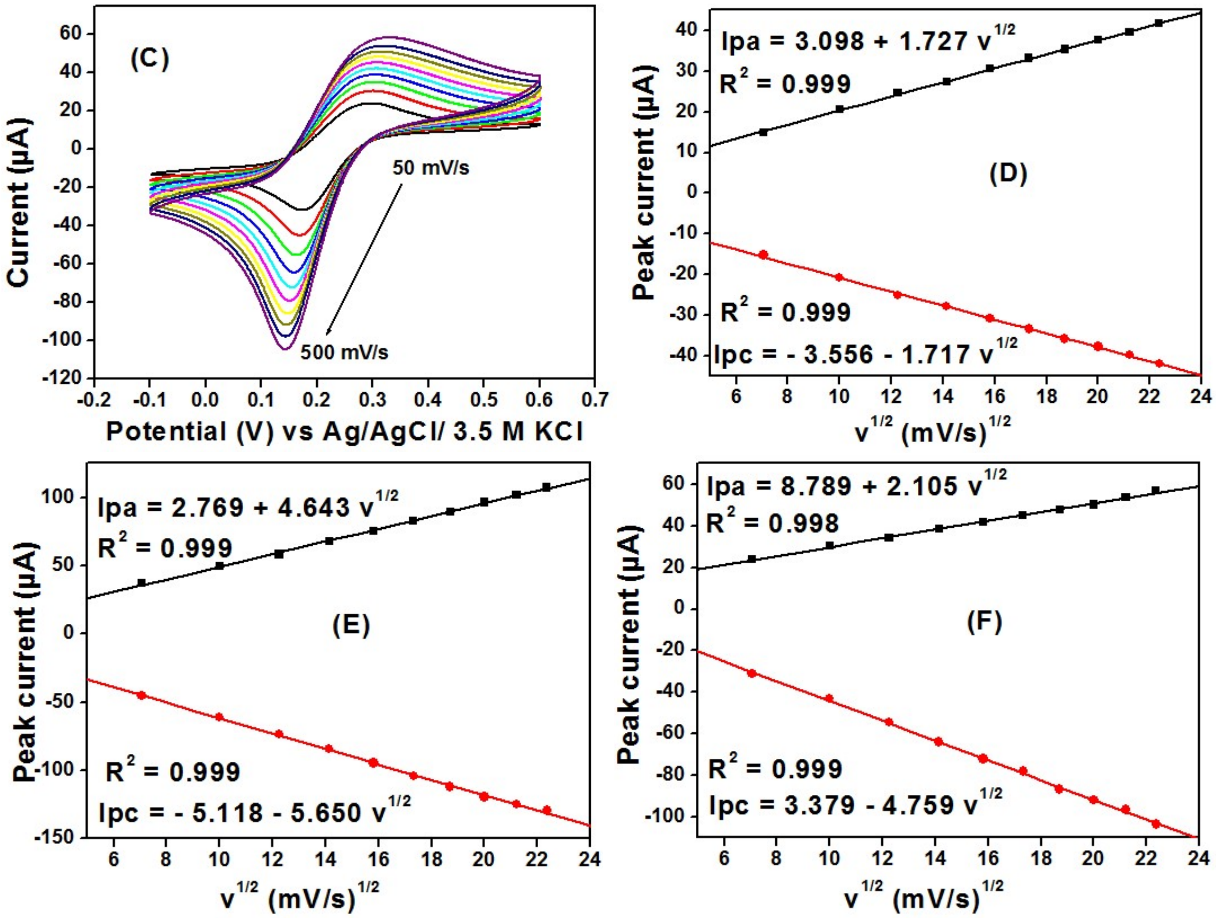

Fig. SF6. Multisweep cyclic voltammograms (A, B and C) and the corresponding peak current versus the root square of the scan rate (D, E and F) respectively for bare Pt, Fc/FMWCNT-POF/Pt and UOx/Fc/FMWCNT-POF/Pt recorded in 0.1 M KCl containing 5 mM $[Fe(CN)_6]^{3-/4-}$ at pH 7. The scan rate was 50; 100; 150; 200; 250; 300; 350; 400; 450 and 500 mV/s.

SF7. Optimization of enzyme loading and pH of the buffer

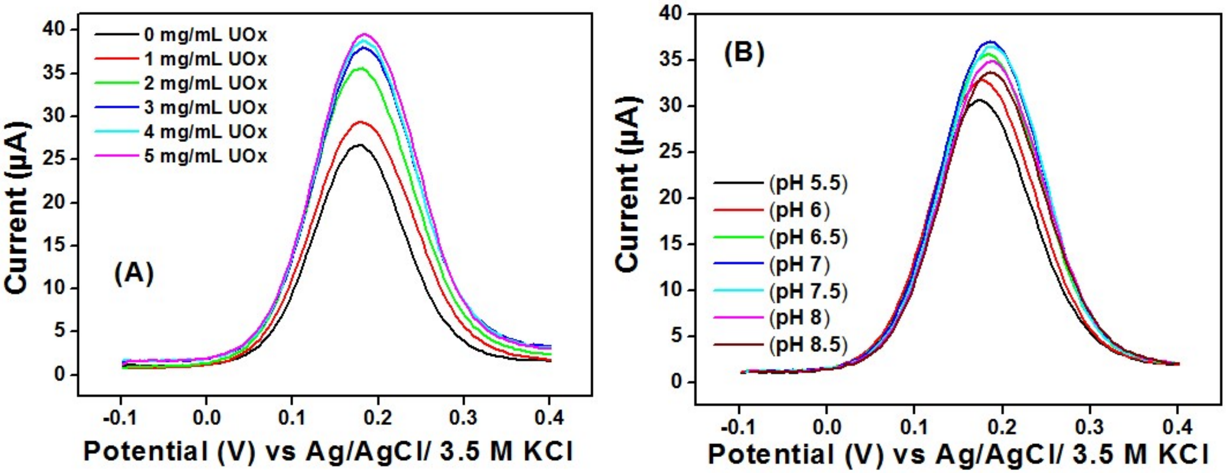

Fig.SF7. (A) DPV response of UOx/Fc/FMWCNT-POF/Pt with different amount of UOx (1-5 mg/mL) in 0.1 M KCl containing 5 mM $[Fe(CN)6]^{3-/4-}$ and 200 µM UA solution pH 7. (**B**) DPV response of UOx/Fc/FMWCNT-POF/Pt biosensor towards different pH of UA solution (5.5-8.5; 200 µM) in 5 mM $[Fe(CN)_6]^{3-/4-}$ containing 0.1 M KCl solution.

SF8. Selectivity

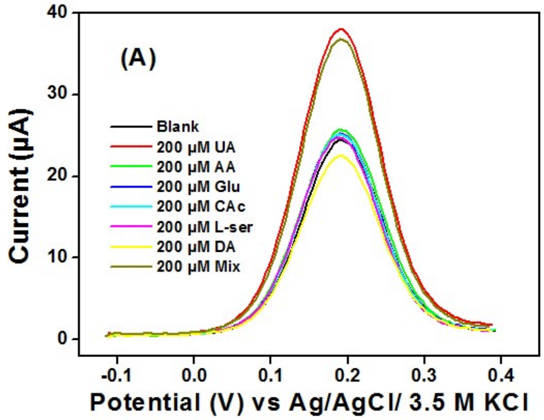

Fig.SF8. DPV responses of UOx/Fc/FMWCNT-POF/Pt in 0.1 M KCl (pH 7) containing 5 mM $[Fe(CN)_6]^{3-/4-}$ in the presence of different interfering-analytes (each 200 µM).

SF9. Reproducibility and repeatability

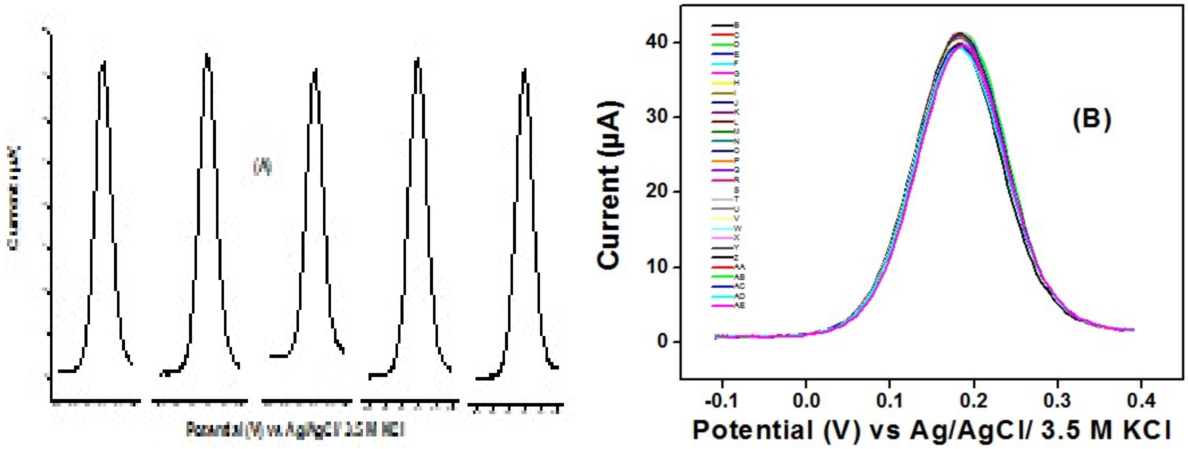

Fig.SF9. DPV responses of UOx/Fc/FMWCNT-POF/Pt in 0.1 M KCl (pH 7) containing 5 mM $[Fe(CN)_6]^{3-/4-}$ in the presence of 200 µM UA for (A) five different fabrication of the biosensor, and (B) for 30 repeated scan with the same biosensor.

SF10. Stability

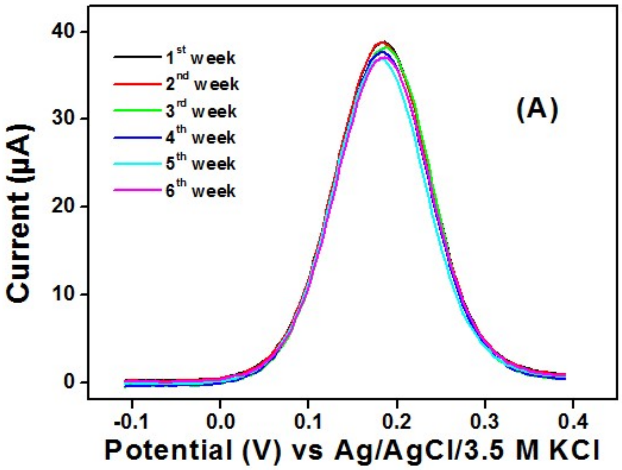

Fig. SF10. Differential pulse voltammograms responses of UOx/Fc/FMWCNT-POF/Pt in 0.1 M KCl (pH 7) containing 5 mM $[Fe(CN)_6]^{3-/4-}$ in the presence of 200 µM UA for (A) stability.

References

[1] N. Chauhan and C. S. Pundir, An amperometric uric acid biosensor based on multiwalled carbon nanotube-gold nanoparticle composite, Anal. Biochem., 2011, **413**, 97-103.

[2] M. C. D. Ngaha, V. K. Tchieda, A. K. Tamo, G. Doungmo, E. Njanja and I. K. Tonle, Aminoalcohol-functionalization of Alkali Palm Oil Fiber and Application as Electrochemical Sensor for 2-nitrophenol Determination, *Electroanalysis*, 2022, **34**, 1-14.

[3] P. G. Seligra, F. Nuevo, M. Lamanna and L. Famá, Composites: Part B. Covalent grafting of carbon nanotubes to PLA in order to improve compatibility, *Compos. B. Eng*., 2013, **46**, 61-68.

[4] D. Vennerberg, R. Hall and M. R. Kessler, Supercritical carbon dioxide-assisted silanization of multi-walled carbon nanotubes and their effect on the thermo-mechanical properties of epoxy nanocomposites, *Polymer*, 2014, **55**, 4156-4163.

[5] K. Jindal, M. Tomar and V. Gupta, CuO thin film based uric acid biosensor with enhanced response characteristics, *Biosens. Bioelectron*., 2012, **38**, 11-18.

[6] B. Wu, L. Xiao, M. Zhang, C. Yang, Q. Li, G. Li, Q. He, and J. Liu, Facile synthesis of dendritic-like CeO_2/rGO composite and application for detection of uric acid and tryptophan simultaneously, J. Solid State Chem., 2021, **296**, 122023.